

## Article (refereed) - postprint

---

Lin, Xiaodan; Yu, Shen; Yang, Dawen; Hutchins, Michael G. ; Ding, Jing; Hong, Bing; Chen, Peiji; Liu, Xun. 2020. **Discriminating surface soil inorganic nitrogen cycling under various land uses in a watershed with simulations of energy balanced temperature and slope introduced moisture.**

© 2020 Elsevier B.V.

This manuscript version is made available under the CC BY-NC-ND 4.0 license  
<https://creativecommons.org/licenses/by-nc-nd/4.0/>



This version is available at <https://nora.nerc.ac.uk/id/eprint/527509>

Copyright and other rights for material on this site are retained by the rights owners. Users should read the terms and conditions of use of this material at <https://nora.nerc.ac.uk/policies.html#access>.

**This is an unedited manuscript accepted for publication, incorporating any revisions agreed during the peer review process. There may be differences between this and the publisher's version. You are advised to consult the publisher's version if you wish to cite from this article.**

The definitive version was published in *Journal of Hydrology*, 587, 124950. 13, pp. [10.1016/j.jhydrol.2020.124950](https://doi.org/10.1016/j.jhydrol.2020.124950)

The definitive version is available at <https://www.elsevier.com/>

Contact UKCEH NORA team at  
[noraceh@ceh.ac.uk](mailto:noraceh@ceh.ac.uk)

**Discriminating surface soil inorganic nitrogen cycling under various land uses in a watershed with simulations of energy balanced temperature and slope introduced moisture**

Xiaodan Lin<sup>a,b</sup>, Shen Yu<sup>a,\*</sup>, Dawen Yang<sup>c</sup>, Michael G. Hutchins<sup>d</sup>, Jing Ding<sup>a</sup>, Bing Hong<sup>a</sup>, Peiji Chen<sup>a,b</sup>, Xun Liu<sup>a,b</sup>

<sup>a</sup>CAS Key Laboratory of Urban Environment and Health, Institute of Urban Environment, Chinese Academy of Sciences, Xiamen 361021, China.

<sup>b</sup>University of Chinese Academy of Sciences, Beijing 100049, China.

<sup>c</sup>Tsinghua University, Beijing 100084, China

<sup>d</sup>Centre for Ecology and Hydrology, Oxfordshire, OX10 8BB, UK

**Corresponding author:**

Shen Yu

CAS Key Laboratory of Urban Environment and Health

Institute of Urban Environment

Chinese Academy of Sciences

1799 Jimei Road

Xiamen 361021

China.

Email: [syu@iue.ac.cn](mailto:syu@iue.ac.cn)

**Abstract**

Surface soil under various land uses/covers plays an important pool of N discharge in a watershed. Soil temperature and moisture drive soil N cycling, especially important for the watersheds with anthropogenic manipulations. Not all of the ongoing process-based models consider topographic factors of known importance when simulating soil moisture but most of them simulate soil temperature typically derived from empirical relations with air temperature. These assumptions might lead to underestimate the N discharge in the watersheds. This study employed an energy balanced soil temperature module and a slope introduced soil moisture module in coupling with a conceptual model of hydro-bio-geochemical process-based watershed life cycle analysis, i.e. the Watershed Inorganic Nitrogen Dynamic (WIND), to simulate soil N cycling across forest land, farmland, and urban bare land in an urbanizing watershed in southern China. The model was calibrated and validated by two individual survey events in 2013 and 2016-17 respectively using moisture and inorganic N in surface soil (0-10 cm) of the watershed with determination coefficients ( $R^2$ ) above 0.7. Significantly higher soil temperature arose when using the energy balanced module in comparison to the air temperature module. Meanwhile, soil moisture declining with land slope became significant above 15° steepness. Estimates of surface soil N cycling across all

land uses were significantly altered. Importantly, land uses determined the extents of their alterations. The WIND provides insights into drivers of hot - spot/hot - moment hydro-bio-geochemical processes of soil inorganic N for land uses in the watershed. More generally, as the findings inform a better constraint of parameters in other physics-based watershed-scale water quality models they also potentially directly contribute to improved strategies for sustainable management of inorganic N discharges under the predicted climate changes.

*Keywords:* Inorganic N dynamics; Surface soil; Dynamic life cycle analysis; Soil moisture; Land use type; Watershed

## 1. Introduction

Nitrogen (N) is one of the essential elements stabilizing natural ecosystems (Vitousek and Howarth, 1991). Human activities, however, have dramatically altered the global N cycle with increasing N loads in the environment (Galloway and Cowling, 2002). Nitrogen in surface soil of various land use types serves as a source of N loading in the aquatic ecosystem of a watershed (Gao et al., 2013). Excess N from surface soil with increasing anthropogenic N inputs (e.g., extensive N deposition and N fertilization) have caused serious ecological and environmental problems in watersheds, including greenhouse gas emission (Congreves et al., 2016) and water eutrophication (Kaushal et al., 2011), threatening the watershed sustainability and eventually putting human health at risk. The N source-sink complexity in a watershed can be elaborated by water confluence via integrating spatiotemporal distribution of N loading, hydrological regime, soil physicochemical properties, and biogeochemical processes (Lin et al., 2018). Understanding how to best manipulate the N source-sink relationship is of considerable concern for water quality and watershed sustainable management worldwide (Congreves et al., 2016).

Besides N substrates, N biogeochemical processes are highly regulated by environmental abiotic factors, such as soil temperature and moisture (Yu and Ehrenfeld, 2010; Ehrenfeld and Yu, 2012; Ahmed et al., 2019; Morugan-Coronado et al., 2019). For example, potentials of biological N fixation and denitrification in orchard soils were improved by increased soil moisture in the proximity of the dripping irrigation (Morugan-Coronado et al., 2019). Soil moisture, in turn, has a dynamic relationship with soil temperature, partitioning energy and radiation that reach land surface (Berg et al., 2014; Hauser et al., 2016). Surface soil moisture is, on the other side, highly influenced by land slope (Qiu et al., 2001) which determines the routing of water either infiltrating the soil profile or as surface runoff during rainfall or irrigation events. In other words, the land slope changes soil moisture and runoff hydrological regime simultaneously (Stieglitz et al., 2003; Vaezi et al., 2017). Steep

topography can result in rapid surface runoff and considerable subsurface drainage, which lead to substantial N loss into watershed aquatic ecosystems (Wu et al., 2018).

Numerous process-based models have been used to track N dynamics at a watershed scale, including the Agricultural Nonpoint Source Pollution (AGNPS/AnnAGNPS; Li et al., 2015), the Soil-Water-Plant-Drainage Systems (SWPD; Matinzadeh et al., 2017), the Soil and Water Assessment Tool (SWAT; Arnold et al., 2012), the Model of Acidification of Groundwater in Catchments (MAGIC; Oulehle et al., 2012), and the Integrated Nitrogen in Catchments (INCA; Wade et al., 2002). Among them, soil N biogeochemical processes are highly considered and incorporated with distributed hydrological models, such as SWAT, INCA, and AnnAGNPS. The existing watershed N dynamic models provide comprehensive simulations on water and N movements but simplify soil N biogeochemical processes in various ways, such as AnnAGNPS only including mineralization and denitrification processes, and INCA and SWAT with mineralization, nitrification, and denitrification processes (Costa et al., 2020). Meanwhile, soil temperature and moisture are critical factors of soil N biogeochemical processes (Agehara and Warncke, 2005; Butterbach-Bahl et al., 2013) as well as hydrological processes (Nanda et al., 2019). Simulations on soil temperature and moisture are diverse among these existing models as well. Except the SWAT and AnnAGNPS, most of the watershed N dynamic models seldom consider the indirect effect of land slope on soil moisture, not even on associated N dynamic processes although its effect on hydrological regime has been well recognized (Wade et al., 2002). Soil temperature, however, is included in most of the process-based models for soil hydro-thermal processes, soil mass transportation, soil structure, and soil microbes mediating N processes (Agehara and Warncke, 2005; Butterbach-Bahl et al., 2013; Costa et al., 2020; Zhao et al., 2020). Given constraints of scaling up field observations tempo-spatially to a watershed scale, soil temperature has often been simulated by a variety of empirical approaches mainly using air temperature (Bai et al., 2014; Huang et al., 2018a). For instance, INCA uses a sine function of air temperature and average annual temperature amplitude to simulation soil temperature, and SWAT uses weighting functions based on average annual air temperature and current day's soil surface temperature (Costa et al., 2020; Wade et al., 2002). Kwon and Koo (2017) found that surface soil temperature was simultaneously determined by air temperature and solar radiation and the air temperature only empirical models led to soil temperature consistently lower than air temperature. However, the field measurement found that surface soil temperature was higher than the air temperature during the daylight time (Qi et al., 2019). Energy balance models with solar radiation further revealed that soil temperature is correlated to soil moisture and heat flux (Herb et al., 2008; Kettridge and Baird, 2008). On the other side, land use/cover type

determines an intensity of solar radiation to reach surface soil (Herb et al., 2008). Therefore, the air-temperature based simulation might lead to underestimates of surface soil temperature, in turn which might further impede the accuracy of the above-mentioned various models in simulating N cycling in a watershed with mixed land use/cover.

As fundamental parameters in controlling watershed N cycling, accuracy of soil temperature and soil moisture simulations is of fundamental importance for the model output. This study developed a slope-introduced soil moisture module and an energy-balanced soil temperature module to integrate a watershed inorganic N dynamic (WIND) model, materialized from the hydro-bio-geo-chemical process-based LCA conceptual model (Lin et al., 2018). The WIND model was calibrated and validated by two field survey events in 2013 and 2016-2017 respectively in an urbanizing watershed in Xiamen, southeastern China. With the energy-balanced soil temperature and the slope-introduced soil moisture, the WIND model is hypothesized to delineate differences of N cycling processes across various land use/cover types (i.e. forest, farmland, and urban bare land) in the studied watershed except their differences from the empirical air temperature-based soil temperature routine and non-slope introduced soil moisture (i.e. the slope at 0°). Meanwhile, rates of the N cycling processes in surface soil from the studied watershed were freshly measured by a consecutive N transformation approach (i.e. mineralization, nitrification, and denitrification) using urea as the only N source instead of the traditional and individual substrate enriched potential methods. It assumed to provide “real” parameters for the simulations. Findings from this study will contribute strategies and tools for sustainable watershed N cycle via manipulating hot spot - hot moment of N source - sink relationships (Groffman et al., 2002) to mitigate against their adverse effects under the predicted global warming.

## **2. Materials and methods**

### *2.1. Study region*

An urbanizing watershed, the Bantou Reservoir watershed in Jimei District, Xiamen, southeastern China, was chosen to test the hypotheses (24°39'12" N, 118°0'58" E; Fig. 1). The study watershed has two cascading reservoirs as headwaters built in 1957 for an agricultural irrigation purpose and shifted as a drinking water source for the Xiamen municipal since 2002. The watershed covers approximately 205 km<sup>2</sup> and is characterized by the Asian Subtropical Monsoon Climate with a mean annual precipitation of 1,462 mm and a mean annual daily temperature of 22°C during 2013 - 2017. An obvious urbanization in the watershed started since 2005 according to the

time-series satellite image interpretation. The watershed is dominated by lateritic soil and is consisted of four types of the 1<sup>st</sup> categorical land uses interpreted in 2013 and 2017, as farmland (mainly vegetable and orchard upland, 108 patches with median size of 0.21 km<sup>2</sup> and 22.3 km<sup>2</sup> in total), forest land (mainly mature and full canopy pine forest, 5 patches with median 6.08 km<sup>2</sup> and 90.8 km<sup>2</sup> in total), urban land (impervious surfaces and bare land (permeable surface), 320 patches with median 0.02 km<sup>2</sup> and 70.9 km<sup>2</sup> in total) and water surface. Slope of land use patches differs among the land use types, i.e. 2 - 30° (median at 15°) for forest land patches, 0 - 27° (median at 5°) for farmland patches, and 0 - 12° (median at 5°) for urban bare land patches, respectively.

## 2.2. Soil sampling and chemical analysis

Surface soil is the most active layer involving input/output of nutrient cycles in a watershed. Two sampling events of surface soil (0 - 10 cm) were undertaken during March - April, 2013 and November 2016 - March, 2017, respectively. In total, 137 sites were sampled from patches of the three land use types (25 surface soil samples from forest land; 49 surface soil samples from farmland; and 63 surface soil samples from urban bare land) for each sampling event (Fig. 1). At each site, five samples were taken from a 10 m × 10 m quadrat and mixed as one composite soil sample. One cutting ring sample for bulk density measurement was randomly selected from the quadrat at each site. All samples were sealed in Ziploc polyethylene bags and transported to the laboratory on ice. Each composite soil sample was divided into three subsamples: one was passed through a Mesh-10 sieve and oven-dried at 105 °C to reach a constant weight for soil moisture measurement; one passed through the Mesh-10 sieve to measured rates of microbial N transformation processes (denitrification, nitrification, and mineralization) in a sealed microcosm incubation system with helium substitution to nitrogen in headspace; the remaining subsample was air-dried and passed through the Mesh-10 and Mesh-100 sieve for chemical analyses.

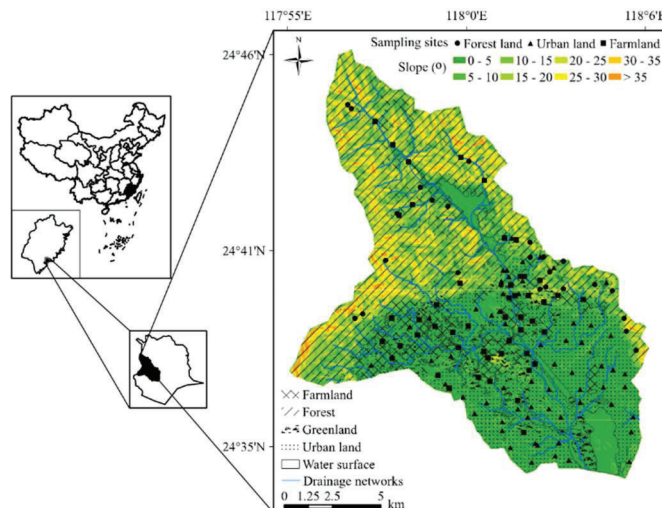


**Fig. 1.** Map of the Bantou Reservoir watershed in Jimei District, Xiamen, China. Slope ranges in color were mapped based on the DEM data. Circles in black indicate surface soil sampling points in forest land, triangles in purple in urban bare land, and squares in pink in farmland. Different patterns represent land use type.

Bulk density was determined by oven-drying the cutting ring samples at 105 °C to reach a constant weight. Total nitrogen (TN) and carbon (TC) in surface soil samples were determined using an element analyzer (Vario MAX, Elementar GmbH, Germany). Nitrate ( $\text{NO}_3^-$ -N) and ammonium ( $\text{NH}_4^+$ -N) were measured in filtrates through a 0.45- $\mu\text{m}$  membrane filter after an extraction with 2 M KCl for one-hour reciprocatory shaking using a flow injection analyzer (FIA QC5000, Lachat, USA). The contents of soil  $\text{NH}_4^+$ -N and  $\text{NO}_3^-$ -N were calculated as mg N per kg oven-dried soil and then converted into  $\text{kg km}^{-2}$  with soil bulk density. The microbial N transformation rates were measured based on aerobic incubation of 10 g homogenized field moisture soil samples in a sealed air-water-soil microcosm. Headspace of the microcosm was vacuumed and flushed 3 times with pure helium gas. One milliliter of urea was injected into each vacuumed microcosm to reach the N content at 1 mg N per microcosm and an equal volume of deionized water was injected into the control microcosm for each surface soil sample. Then, the helium gassed headspace of the microcosm was balanced with a syringe of 50 mL  $\text{O}_2$  by push-and-pull for 5 minutes. The microcosms were incubated in the dark for 72, 96, and 120 hours at room temperature. The headspace air of the timed microcosms was then determined for  $\text{N}_2$ ,  $\text{N}_2\text{O}$ ,  $\text{CO}_2$ , and  $\text{CH}_4$  using a gas chromatography system (Agilent® 7890A, Agilent Technologies, Santa Clara, CA, USA) equipped with a capillary column (HP-5, 30-m long with internal diameter of 0.32-mm and film thickness of 0.25- $\mu\text{m}$ ) and an electron capture detector (ECD). Then the microcosms were injected with 40 mL 2M KCl and one-hour reciprocatory shaking. The supernatant was filtered through a 0.45- $\mu\text{m}$  membrane filter and the filtrates were analyzed for  $\text{NH}_4^+$ -N and  $\text{NO}_3^-$ -N using the flow injection analyzer (FIA QC5000, Lachat, USA).

### 2.3. Data preparation

Interpretation of land use/land cover into forest, farmland, urban land, and water surface was initially done visually on the Landsat ETM+ images in August 2010, downloaded from the Geospatial Data Cloud Site at the Computer Network Information Center, Chinese Academy of Sciences at <http://www.gscloud.cn/>. The land use /land cover changes were corrected with the ETM+ images and field visits in 2013 and 2017. Slope of the watershed was extracted from the GDEM V2 data at the Geospatial Data Cloud Site website with a 30-m resolution. Meteorological data were downloaded from the National Meteorological Information Center at <http://data.cma.cn>. The detailed sources of parameters and datasets for the simulations were listed in Table 1.

### 2.4. Model description

The conceptual diagram of Watershed Inorganic Nitrogen Dynamic (WIND) model was depicted as a putative network of N dynamic life cycle in a watershed (Fig. 2, Zhao et al., 2011; Lin et al., 2018). The WIND model simulated daily changes in

inorganic N ( $\text{NH}_4^+\text{-N}$  and  $\text{NO}_3^-\text{-N}$ ) dynamics in surface soil under three land uses (forest, farmland, and urban bare land uses). Briefly, external inputs of soil inorganic N include atmospheric deposition, lightning  $\text{N}_2$  fixation, and fertilization while internal transformations of soil N are assumed mostly as mineralization of organic N into  $\text{NH}_4^+$ , which is thereafter taken up by plants and lost via  $\text{NH}_3$  volatilization, surface runoff and infiltration, or oxidized into  $\text{NO}_3^-$  through nitrification under aerobic condition.  $\text{NO}_3^-$  can be also taken up by plants, exported via surface runoff and infiltration to surface and ground water, or returned to the atmosphere by denitrifiers under hypoxic or anaerobic condition (Fig. 2). Mathematical equations of these mentioned processes in the WIND model were labeled in Fig. 2 and detailed in Table S1 with parameters in Table S2 of the Supplementary Materials.

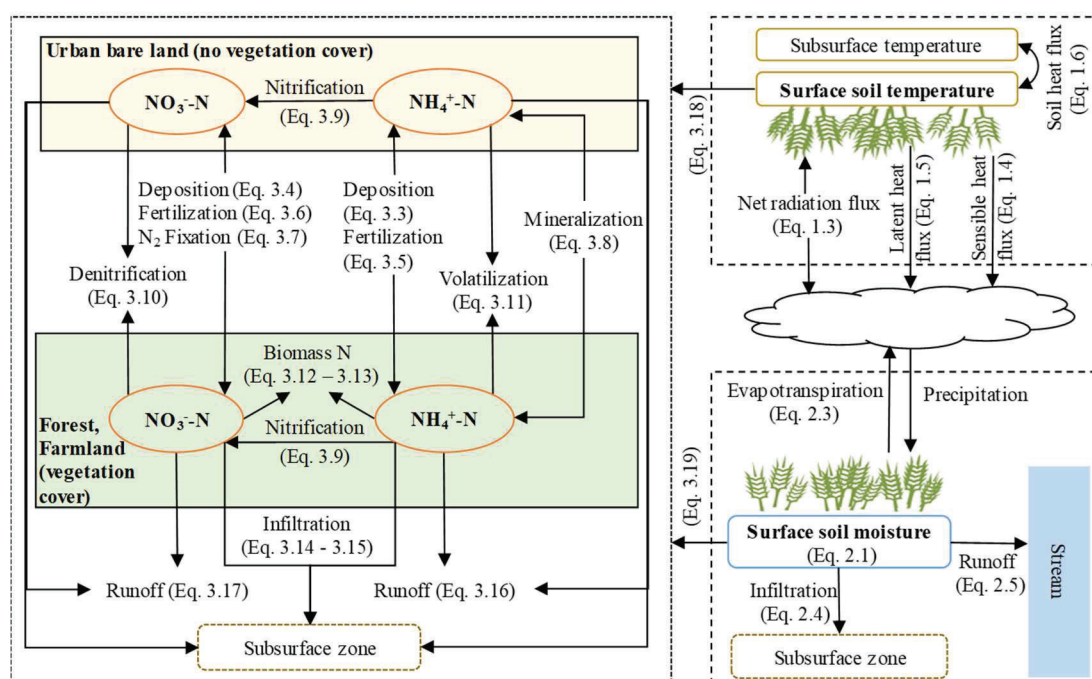


**Fig. 2.** Conceptual diagram for the Watershed Inorganic Nitrogen Dynamic (WIND) Model. Energy balanced soil temperature module (the upright frame) and slope introduced soil moisture module (the downright frame) are employed to estimate soil temperature and soil moisture in surface soil of forest land, farmland, and urban bare land uses. The adjusted soil temperature and soil moisture were used to simulate changes of inorganic N dynamic processes in surface soil of three land use types. Corresponding equations can be found in Table S1 by the equation number near the arrows.

An energy-balanced soil temperature module (EnTemp, Fig. 2, the upper right frame) and slope-introduced soil moisture module (SMoist, Fig. 2, the lower right frame) were included in this study to simulate inorganic N cycling in surface soil under different land use types, i.e. forest land, farmland, and urban bare land. The simulated results were compared with those by air temperature-based soil temperature module (AirTemp) and slope-introduced soil moisture module when slope equals  $0^\circ$  (NSMoist). The energy-balanced soil temperature module includes net radiation flux, sensible heat flux, latent heat flux, and soil heat flux (Kwon and Koo, 2017) detailed

in Fig. 2 and Table S1 (Eqs. 1.1 - 1.6), incorporated with topography and land use type, soil moisture, air temperature, and rainfall (Table S2). The empirical soil temperature module, i.e. air temperature-based module (AirTemp), is adopted from Wade et al. (2002) with details in Table S1 (Eq. 1.7). Meanwhile, the slope-introduced soil moisture module includes rainfall, evapotranspiration (moisture from soil to air pathway), infiltration, and surface runoff (Fig. 2 and Table S1, Eqs. 2.1 - 2.5; Fox et al., 1997; Allen et al., 1998; Huang et al., 2016). The median patch slope (°) of each land use type in the watershed was used for simulation. The daily rainfall volume (mm) was set from 0 mm to the maximum daily rainfall volume during the studied period of 2013-2017. The slope-introduced daily soil moisture was simulated as well. Then,  $\text{NH}_4^+\text{-N}$  and  $\text{NO}_3^-\text{-N}$  in surface soil (0-10 cm) of the three land use types were simulated by a mass balance method with the simulated soil temperature and moisture as Eqs. 1 - 2 and Table S1 (Eqs. 3.3 - 3.21; Zhao et al., 2011). The dynamic balances of inorganic N cycling among sources, sinks, and transport/transformation processes over time were conducted in a dynamic modelling software package of iThink and STELLA (Ver. 9.1.3, [www.iseesystems.com](http://www.iseesystems.com)).

$$\frac{d\text{NH}_4^+}{dt} = \text{NH}_{dep} + \text{NH}_{fer} + \text{NH}_{min} - \text{NH}_{nit} - \text{NH}_{vol} - \text{NH}_{upt} - \text{NH}_{inf} - \text{NH}_{run} \quad (1)$$

$$\frac{d\text{NO}_3^-}{dt} = \text{NO}_{dep} + \text{NO}_{fer} + \text{NO}_{fix} + \text{NH}_{nit} - \text{NO}_{den} - \text{NO}_{upt} - \text{NO}_{inf} - \text{NO}_{run} \quad (2)$$

Where  $\frac{d\text{NH}_4^+}{dt}$  and  $\frac{d\text{NO}_3^-}{dt}$  represent daily mass rates of  $\text{NH}_4^+$  and  $\text{NO}_3^-$ ;  $\text{NH}_{dep}$  and  $\text{NO}_{dep}$  represent daily atmospheric deposition rates of  $\text{NH}_4^+$  and  $\text{NO}_3^-$ ;  $\text{NH}_{fer}$  and  $\text{NO}_{fer}$  represent daily average input rates of  $\text{NH}_4^+$  and  $\text{NO}_3^-$  fertilizers;  $\text{NH}_{min}$  represents daily mineralization rate;  $\text{NH}_{vol}$  represents daily  $\text{NH}_4^+$  volatilization loss rate;  $\text{NH}_{nit}$  represents daily  $\text{NH}_4^+$  nitrification rate;  $\text{NO}_{fix}$  represents daily lightning  $\text{NO}_3^-$  fixation rate;  $\text{NO}_{den}$  represents daily  $\text{NO}_3^-$  denitrification loss rate;  $\text{NH}_{upt}$  and  $\text{NO}_{upt}$  represent plant uptake rates of  $\text{NH}_4^+$  and  $\text{NO}_3^-$ ;  $\text{NH}_{inf}$  and  $\text{NO}_{inf}$  represent daily filtration loss rates of  $\text{NH}_4^+$  and  $\text{NO}_3^-$ ;  $\text{NH}_{run}$  and  $\text{NO}_{run}$  represent daily surface runoff loss rates of  $\text{NH}_4^+$  and  $\text{NO}_3^-$ , respectively. All the rates were expressed with a unit of  $\text{kg N km}^{-2} \text{ day}^{-1}$ .

All of the parameters of the WIND model were listed in Table S2.

### 2.5. Model calibration and validation

For both configurations of the WIND model the parameter sets consisting of 12 parameters for soil water balances and 22 parameters for soil inorganic N dynamic balances were manually calibrated and validated against the soil measurement data from 2013 and 2016/2017, respectively (Table S2). The parameters (plant potential factor, model coefficient of runoff generation and infiltration rate) used for simulating soil moisture of each land use type were collected from literatures, while maximum

water storage used for simulating the soil moisture of each land use type were based on the measurements of this study. The parameters (mineralization, nitrification and denitrification rates) used for simulating the soil inorganic N cycling of each land use type according to the measurement of this study but rates of volatilization, deposition, and plant uptake rates were collected from literatures. More detailed parameters of the WIND model can be found in [Table S2](#).

The WIND model parameters with both corresponding determination coefficient ( $R^2$ ) and a Nash-Sutcliffe efficiency ( $NS$ ) values greater than 0.7 were selected during the calibration with the measurement datasets in 2013 and model performance for the three land use types were evaluated during the WIND model validation by the measurement dataset in 2016/2017. Akaike information criterion ( $AIC$ ) index and sum of  $R^2$  and  $NS$  ( $F$ ) were calculated for the model performance evaluations. The  $R^2$ ,  $NS$ ,  $F$ , and  $AIC$  were calculated as following equations,

$$R^2 = \left( \frac{\sum(obs - \Delta obs) \times (sim - \Delta sim)}{\sqrt{\sum(sim - \Delta sim)^2} \times \sqrt{\sum(obs - \Delta obs)^2}} \right)^2 \quad (3)$$

$$NS = 1 - \frac{\sum(sim - obs)^2}{\sum(obs - \Delta obs)^2} \quad (4)$$

$$F = R^2 + NS \quad (5)$$

$$AIC = n \ln \left( \frac{RSS}{n} \right) + 2k \quad (6)$$

Where  $sim$  and  $obs$  represent the simulated and observed values, respectively, while  $\Delta obs$  is an average of the observed values and  $\Delta sim$  is an average of the simulated values.  $RSS$  is the residual sum of squares of the model,  $n$  is the sample size and  $k$  is the number of fitted parameters in the model.

## 2.6. Statistical analysis

Data were transformed using a Box-Cox method to meet the normality using Shapiro-Wilk test. The t - test was employed to explore statistical significance of differences in daily surface soil temperature between EnTemp and AirTemp, and daily inorganic N pool in surface soil between the two soil temperature simulations in the period of 2013-2017. One-way analysis of variance (ANOVA) was carried out for soil moisture and inorganic N pool in surface soil along a land slope gradient of 0°-30° for each land use type with Tukey's post hoc test (significance level alpha = 0.05) while N-way ANOVA was applied to testify effects of land use types and the land slope gradient (significance level alpha = 0.05). Multiple linear regression analysis was used to explore the contributions of soil moisture and temperature to the daily changes of inorganic N pools, N cycling processes' rates, and N loss rates in surface soil of forest land, farmland, and urban bare land uses. The 'circlize' package in R was used to construct "circo plot" of each land use to analyze the input, output, and

transport/transformation pathways of N. All statistical analyses were carried out in the R system (Version 3.5.1, The R Foundation for Statistical Computing).

### 3. Results

#### 3.1. Performance of the WIND model and slope-introduced soil moisture module

The validated WIND model with the energy-balanced daily soil temperature (EnTemp) module and the slope-introduced daily soil moisture (SMoist, a median slope at 15° for forest land and 5° for farmland and urban bare land, respectively) module demonstrated promising performance (Fig. 3 upper) with better fitness of the validations (red line, all  $F$  values above 1.6 and slight small  $AIC$  values) for inorganic N pools in surface soil than the ones with the air temperature-based daily soil temperature (AirTemp) and soil moisture at slope of 0° (NSMoist) (black line,  $F$  values ranging from 1.063 to 1.669 and slight large  $AIC$  values). Both inorganic N forms ( $\text{NH}_4^+$ -N or  $\text{NO}_3^-$ -N) in the three land use types showed the same trend. Evident difference between combined daily soil temperature and soil moisture was found for  $\text{NH}_4^+$ -N in farmland and for  $\text{NO}_3^-$ -N in urban bare land (Fig. 3 upper), suggesting inorganic N cycling in different land use types might have differing sensitive processes to soil temperature and moisture.

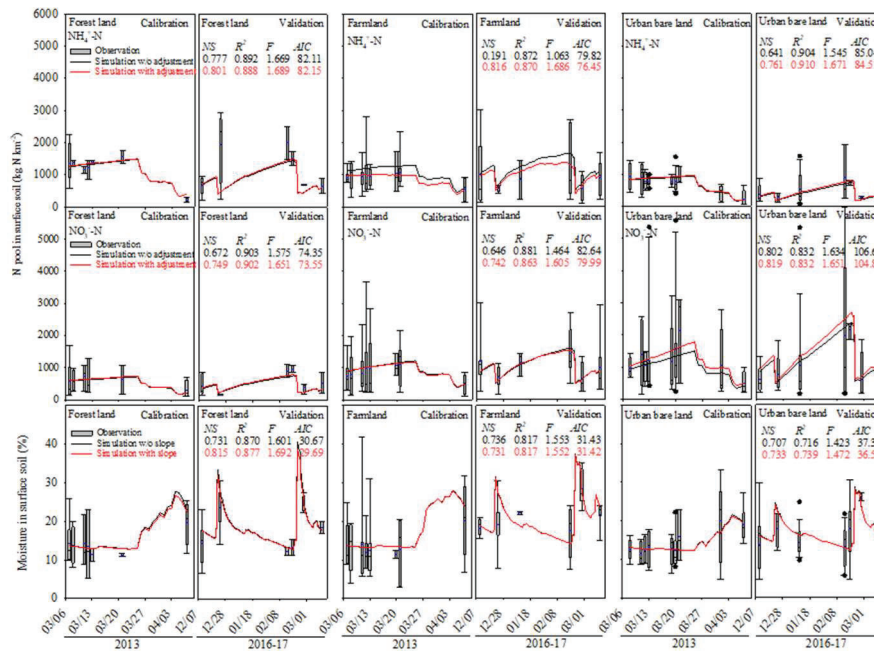


**Fig. 3.** Fitness of the Watershed Inorganic Nitrogen Dynamic (WIND) model on soil inorganic N pool ( $\text{NH}_4^+$ -N and  $\text{NO}_3^-$ -N, upper) and of the slope-introduced soil moisture (SMoist) module on soil moisture (lower) under forest land, farmland, and urban bare land use types in an urbanizing watershed, Xiamen, China. The WIND model and SMOist module were calibrated with the 2013 field measurement dataset and validated by the 2016-2017 field measurement dataset. The line in red (i.e. with adjustment) represents the simulation results using energy - balanced soil temperature (EnTemp) and SMOist while the black line (i.e. w/o adjustment) is simulated by air temperature - based soil temperature (AirTemp) and soil moisture at slope of 0° (NSMoist). A median slope of each land use type was applied for the soil moisture calibration and validation, i.e. 15° for the forest land, and 5° for farmland and urban bare land.

The slope-introduced soil moisture module also had good validation fitness for surface soil moisture of the three land use types ( $F$  values: forest land (1.692) > farmland (1.552) > urban bare land (1.483) and  $AIC$  values: forest land (29.69) < farmland (31.42) < urban bare land (36.57), Fig. 3 lower). The large difference of  $F$  values and  $AIC$  values of soil moisture simulation between the median slope and  $0^\circ$  slope was found in forest land ( $F = 1.692$  versus 1.601,  $AIC = 30.67$  versus 29.69) and urban bare land ( $F = 1.472$  versus 1.423,  $AIC = 37.37$  versus 26.57) while the farm land had similar fitness ( $F = 1.55$  and  $AIC = 31.4$ , Fig. 3 lower), suggesting that land use/cover and topological condition might influence soil moisture.

### 3.2. Slope Effect on soil moisture and inorganic N pools in surface soil of various land use types

The three land use types showed a similar declining pattern of daily soil moisture under daily rainfall in 2013-2017 along the land slope gradient of  $0^\circ$  to  $30^\circ$ , simulated by the slope - introduced soil moisture module (SMoist, Fig. 4 upper). The daily soil moisture declines with the land slope became significant when daily rainfall volume above 50 mm and the land slope above  $15^\circ$  (urban bare land use even significantly above  $10^\circ$ , Fig. 4 upper) according to ANOVA with Tukey's post hoc test ( $p < 0.05$ ). Under the maximum daily rainfall (173 mm) of 2013-2017, the daily soil moisture declined with land slope from 65 ( $0^\circ$ - $10^\circ$ ) to 41.3 mm ( $30^\circ$ ) for forest land, from 64.7 ( $0^\circ$ ) to 34.5 mm ( $30^\circ$ ) for farmland, and from 54.8 ( $0^\circ$ ) to 24.4 mm ( $30^\circ$ ) for urban bare land (Fig. 4 upper). However, the daily soil moisture without rainfall was relatively stable over the land slope gradient, i.e. soil moisture of forest land and farmland consistently at 13.1 mm and 10.6 mm, respectively while urban bare land had a relatively wide range of soil moisture of 13.8 ( $0^\circ$ ) -11.0 ( $30^\circ$ ) mm (Fig. 4 upper).

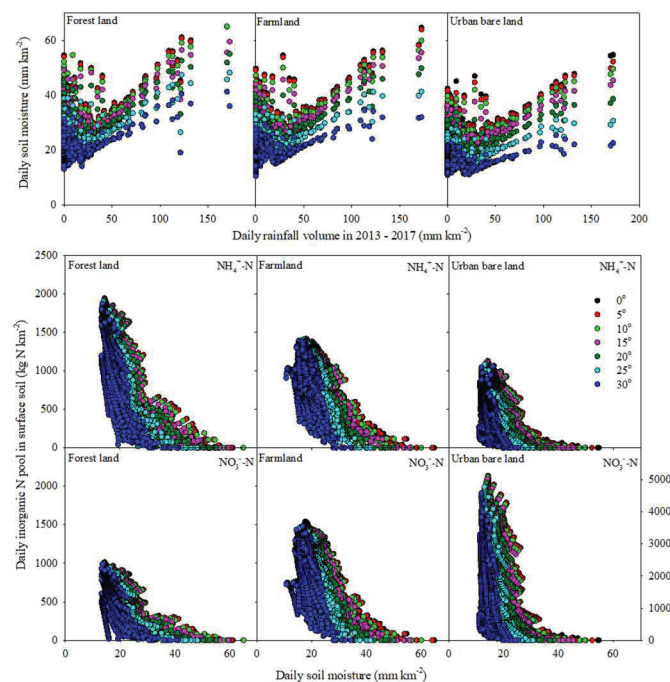


**Fig. 4.** Surface soil moisture changes under forest land, farmland, and urban bare land use types simulated by the slope - introduced soil moisture module in the period of 2013 - 2017 in an urbanizing watershed, Xiamen, China. The slope effect of different land use patch on daily inorganic N pool in surface soil via influencing soil moisture. The  $\text{NO}_3^-$ -N pool had a triple size in urban bare land than in other land use types with an individual scale marked on the right Y axis.

In response to the slope-introduced soil moisture change, inorganic N pools in surface soil showed significant declines with increasing soil moisture but varied with land use type and inorganic N form (Fig. 4 lower). A steep decline of daily inorganic N pools was observed as soil moisture increased from 10 to 40 mm, then gradually down when soil moisture above 40 mm for forest land and farmland and above 30 mm for urban bare land. Similarly, the declines of daily inorganic N pools became quick with land slope increasing from 0° to 30° (Fig. 4 lower). The decrease in median  $\text{NH}_4^+\text{-N}$  for forest land from 907  $\text{kg km}^{-2}$  (0°) to 772  $\text{kg km}^{-2}$  (30°) was greater than for farmland (from 756 to 714  $\text{kg km}^{-2}$ ) and urban bare land (from 425 to 335  $\text{kg km}^{-2}$ ). Whereas, the decrease in median  $\text{NO}_3^-\text{-N}$  for urban bare land from 1323  $\text{kg km}^{-2}$  (0°) to 1038  $\text{kg km}^{-2}$  (30°) was greater than forest land (from 459 to 399  $\text{kg km}^{-2}$ ) and farmland (from 877 to 802  $\text{kg km}^{-2}$ ).

### 3.3. Differences of soil temperature simulated by EnTemp and AirTemp and its effects on inorganic N pools in surface soil of various land use types

Surface soil temperature simulated by the energy-balanced soil temperature module (EnTemp) was significantly higher than when simulated by the air temperature - based soil temperature module (AirTemp) in the period of 2013-2017 with the sampling events (1825 days,  $p < 0.001$ , Fig. 5 upper). The increment of surface soil temperature between EnTemp and AirTemp is dependent upon land use type, i.e. surface soil of urban bare land had a greater increment of soil temperature than those of farmland and forest land. The median increments between EnTemp and AirTemp were 2 °C for forest land, 5 °C for farmland, and 6 °C for urban bare land over the period.

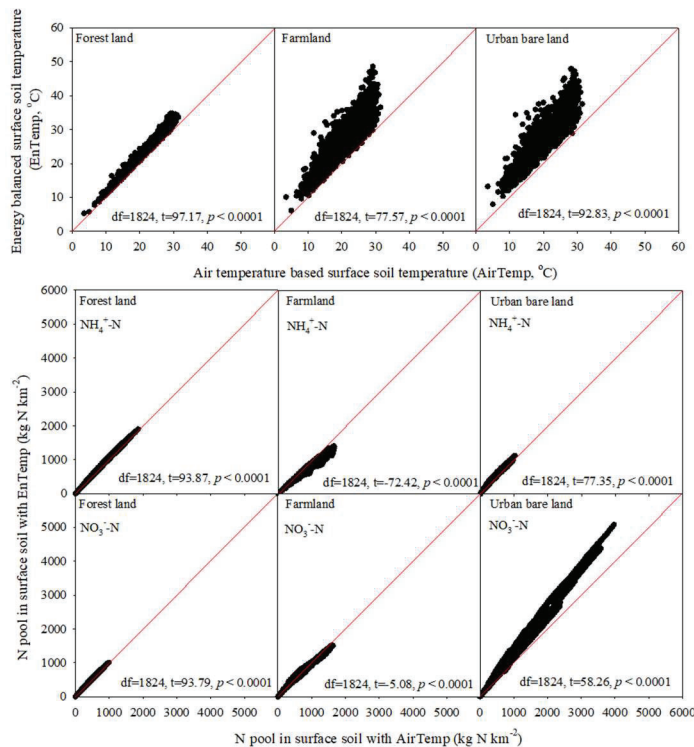


**Fig. 5.** Comparisons between energy - balanced soil temperature (EnTemp) and air temperature - based soil temperature (AirTemp), and their influences on estimates of N pool in surface soil of forest land, farmland, and urban bare land use types in the period of 2013 – 2017 in an urbanizing watershed, Xiamen, China. The solid red line is a diagonal line.

With the increase of soil temperature (EnTemp versus AirTemp) at the median slope of each land use type as above-mentioned, the simulated inorganic N pools in surface soil were significantly but differently shifted by land use type in the period of 2013-2017. Both  $\text{NH}_4^+\text{-N}$  and  $\text{NO}_3^-\text{-N}$  pool sizes were significantly increased in surface soil of forest land and urban bare land but declined in surface soil of farmland with fertilization over the period with EnTemp versus AirTemp (1825 days,  $p < 0.001$ , Fig. 5 lower). The median increment of  $\text{NH}_4^+\text{-N}$  pool size between EnTemp and AirTemp was 2-3 times greater in farmland ( $148 \text{ kg km}^{-2}$ ) than in the forest land ( $50 \text{ kg km}^{-2}$ ) and urban bare land ( $68 \text{ kg km}^{-2}$ ). Whereas, the median increment of  $\text{NO}_3^-\text{-N}$  pool size was the greatest in urban bare land ( $235 \text{ kg km}^{-2}$ ), which was almost 12 times higher than in the forest land ( $19 \text{ kg km}^{-2}$ ) and farmland ( $20 \text{ kg km}^{-2}$ ).

#### 3.4. Nitrogen cycling in surface soil under various land use types of the studied watershed simulated by the WIND model with EnTemp and SMOist modules

Differences in moisture, temperature, inorganic N pool ( $\text{NH}_4^+\text{-N}$  and  $\text{NO}_3^-\text{-N}$ ), multi-process rates of N cycling, and daily N losses in surface soil of the three land use types in the studied watershed were consecutively simulated in the period of 2013-2017 by the WIND model with EnTemp and SMOist modules (Fig. 6). The slope for the SMOist simulation used the median value of each land use type in the watershed, i.e.  $15^\circ$  for forest land,  $5^\circ$  for both farmland and urban bare land. The daily  $\text{NO}_3^-\text{-N}$  pool in surface soil (median at  $1318 \text{ kg N km}^{-2}$ ) was consistently and remarkably greater than the daily  $\text{NH}_4^+\text{-N}$  pool (median at  $423 \text{ kg N km}^{-2}$ ) in the urban bare land (1825 days,  $p < 0.001$ ) while the forest land had a reverse pattern with a nearly double daily pool size of  $\text{NH}_4^+\text{-N}$  (median at  $875 \text{ kg N km}^{-2}$ ) as that of daily  $\text{NO}_3^-\text{-N}$  pool (median at  $446 \text{ kg N km}^{-2}$ ) in surface soil (1825 days,  $p < 0.001$ ). The farmland was balanced with comparative daily pools of  $\text{NH}_4^+\text{-N}$  (median at  $755 \text{ kg N km}^{-2}$ ) and  $\text{NO}_3^-\text{-N}$  (median at  $875 \text{ kg N km}^{-2}$ ) in surface soil. Meanwhile, the urban bare land had the greatest daily  $\text{NO}_3^-\text{-N}$  pool in surface soil among the three land use types in the studied watershed.

Daily rates of N cycling processes, mineralization, nitrification, and volatilization, were significantly shifted with soil temperature (EnTemp) pattern (partial  $R^2$  ranging from 0.117 to 0.937) and slightly integrated with soil moisture (SMOist) pattern (partial  $R^2$  ranging from 0.008 to 0.414, 1825 days,  $p < 0.0001$ , Fig. 6; Table S3). The farmland with fertilization and cropping practices had the most active and diverse N cycling processes, even denitrification, which contributed negligibly to N cycling in upland surface soil of forest land and urban bare land. Daily medians of mineralization, nitrification, volatilization, and denitrification rates in surface soil of the farmland were  $68 \text{ kg N km}^{-2} \text{ day}^{-1}$ ,  $43 \text{ kg N km}^{-2} \text{ day}^{-1}$ ,  $30 \text{ kg N km}^{-2} \text{ day}^{-1}$ , and  $4 \text{ kg N km}^{-2} \text{ day}^{-1}$ , respectively. Daily N cycling in surface soil of forest land was dominated by mineralization (median at  $57 \text{ kg N km}^{-2} \text{ day}^{-1}$ ) and followed by

nitrification (median at  $16 \text{ kg N km}^{-2} \text{ day}^{-1}$ ) and volatilization (median at  $8 \text{ kg N km}^{-2} \text{ day}^{-1}$ ). On the other hand, daily N cycling in surface soil of urban bare land was integratively dominated by mineralization (median at  $43 \text{ kg N km}^{-2} \text{ day}^{-1}$ ) and nitrification (median at  $30 \text{ kg N km}^{-2} \text{ day}^{-1}$ , 1825 days,  $p < 0.001$ , Fig. 6).

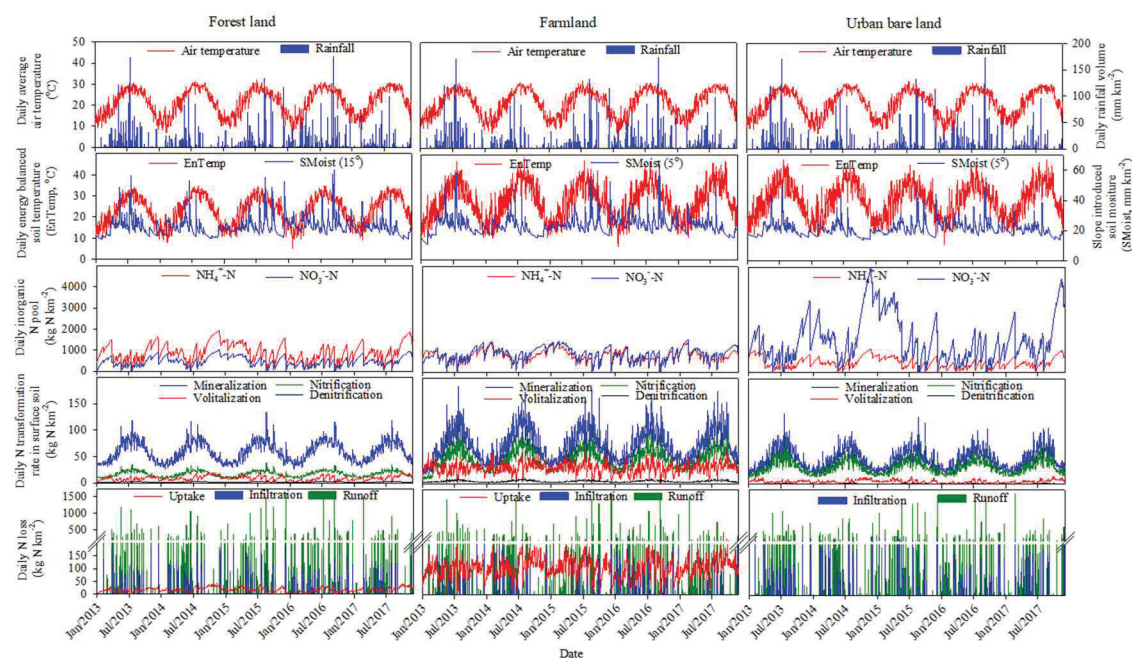


**Fig. 6.** Simulations of the WIND model for daily changes of inorganic N pools, N transformation rates, and N losses in surface soil of forest land, farmland, and urban bare land uses in an urbanizing watershed, Xiamen, China with adjustments of energy - balanced soil temperature and slope - introduced soil moisture. The simulation period covered from 2013 to 2017 when daily average air temperature and rainfall volume were also shown.

Surface runoff was the predominant daily N loss pathway from surface soil, regardless of land use types, with means of  $39 \text{ kg N km}^{-2} \text{ day}^{-1}$  for forest land,  $44 \text{ kg N km}^{-2} \text{ day}^{-1}$  for farmland, and  $57 \text{ kg N km}^{-2} \text{ day}^{-1}$  for urban bare land (Fig. 6).

Vegetation uptake was a considerable daily N loss pathway from surface soil of farmland (median at  $102 \text{ kg N km}^{-2} \text{ day}^{-1}$ ), over 6 times that of forest land (median at  $17 \text{ kg N km}^{-2} \text{ day}^{-1}$ ). Without the vegetation uptake, infiltration became a major pathway of daily N loss from surface soil of urban bare land (median at  $9 \text{ kg N km}^{-2} \text{ day}^{-1}$ ), greater than farmland (median at  $8 \text{ kg N km}^{-2} \text{ day}^{-1}$ ) and forest land (median  $6 \text{ kg N km}^{-2} \text{ day}^{-1}$ ).

Annual N fluxes in surface soil can be classified as input and output for the three land use types in the study watershed (Fig. 7). Except fertilization in farmland, mineralization contributed a profound  $\text{NH}_4^+$ -N input to the inorganic N pool of surface soil, average annual at  $262 \text{ kg N ha}^{-1} \text{ yr}^{-1}$  (54.2% of annual total inorganic N (ATIN) pool) for farmland,  $214 \text{ kg N ha}^{-1} \text{ yr}^{-1}$  (79.7% of ATIN pool) for forest land, and  $169 \text{ kg N ha}^{-1} \text{ yr}^{-1}$  (62.4% of ATIN pool) for urban bare land, which significantly differed among the three land use types ( $p < 0.001$ ,  $n = 5$ , Fig. 7) as the daily mineralization rates mentioned above (Fig. 6). Other sources, such as  $\text{NO}_3^-$ -N air

deposition and  $N_2$  lightning fixation, were important for inorganic N pool in surface soil of urban bare land ( $58.4 \text{ kg N ha}^{-1} \text{ yr}^{-1}$  and 21.5% of ATIN pool, and  $21.9 \text{ kg N ha}^{-1} \text{ yr}^{-1}$  and 8.1% of ATIN pool, respectively) but negligible for forest land and farmland ( $< 12.2\%$  of ATIN pool, Fig. 7). Average annual output flux of  $NO_3^-$ -N via surface runoff was considerably high in urban bare land ( $158 \text{ kg N ha}^{-1} \text{ yr}^{-1}$  and 58.1% of ATIN pool), significantly greater than farmland ( $86 \text{ kg N ha}^{-1} \text{ yr}^{-1}$  and 12.4% of ATIN pool) and forest land ( $47 \text{ kg N ha}^{-1} \text{ yr}^{-1}$  and 17.5% of ATIN pool,  $p < 0.001$ ,  $n = 5$ , Fig. 7). At the same time, surface runoffs also exported  $NH_4^+$ -N annually from surface soil of forest land (mean of  $94 \text{ kg N ha}^{-1} \text{ yr}^{-1}$  and 34.9% of ATIN pool, significantly less than  $NO_3^-$ -N output via surface runoff,  $p < 0.001$ ,  $n = 5$ ), farmland ( $75 \text{ kg N ha}^{-1} \text{ yr}^{-1}$  and 10.8% of ATIN pool), and urban bare land ( $48 \text{ kg N ha}^{-1} \text{ yr}^{-1}$  and 17.7% of ATIN pool), which significantly differed among the land use types ( $p < 0.05$ ,  $n = 5$ ). On the other hand, average annual  $NH_4^+$ -N output via  $NH_3$  volatilization was significantly greater in surface soil of farm land ( $107 \text{ kg N ha}^{-1} \text{ yr}^{-1}$  and 15.6% of ATIN pool), which was over three times of forest land ( $31 \text{ kg N ha}^{-1} \text{ yr}^{-1}$  and 11.8% of ATIN pool) and near 6 times of urban bare land ( $18 \text{ kg N ha}^{-1} \text{ yr}^{-1}$  and 7.1% of ATIN pool, Fig. 7,  $p < 0.001$ ,  $n = 5$ ). Average annual N loss via denitrification was relatively small in comparison with above-mentioned processes,  $16 \text{ kg N ha}^{-1} \text{ yr}^{-1}$  in surface soil of farmland,  $5 \text{ kg N ha}^{-1} \text{ yr}^{-1}$  in surface soil of forest land, and  $3 \text{ kg N ha}^{-1} \text{ yr}^{-1}$  in surface soil of urban bare land, respectively, which were significantly differentiated among land use types ( $p < 0.001$ ,  $n = 5$ ). With vegetation, annual plant uptake accounted for  $202 \text{ kg NH}_4^+$ -N  $ha^{-1} \text{ yr}^{-1}$  and  $175 \text{ kg NO}_3^-$ -N  $ha^{-1} \text{ yr}^{-1}$ , consisting of 36.0%  $NH_4^+$ -N and 59.9%  $NO_3^-$ -N outputs from surface soil of farmland, respectively; while surface soil N in forest land was taken up by plants annually at  $31 \text{ kg NH}_4^+$ -N  $ha^{-1} \text{ yr}^{-1}$  (13.3% of output) and  $32 \text{ kg NO}_3^-$ -N  $ha^{-1} \text{ yr}^{-1}$  (34.6% of output, Fig. 7).

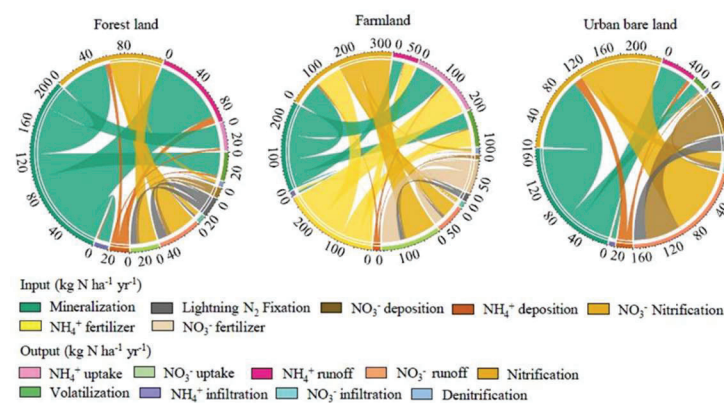


**Fig. 7.** Average annual fluxes of N inputs and outputs in surface soil of forest land, farmland, and urban bare land uses in an urbanizing watershed, Xiamen, China between 2013 - 2017 simulated by the WIND model with adjustments of energy - balanced soil temperature and slope - introduced soil moisture (15° of median slope for forest land use and 5° of median slope for both farmland and urban bare land uses).

#### 4. Discussion

As hypothesized that nitrogen in surface soil (0 - 10 cm) is actively involved in watershed N cycle, the WIND model, with EnTemp and SMOist modules, evidently

differentiates the inorganic N pool of surface soil under three land use types not only in speciation and flux but also in process and process-based annual contribution to inorganic N cycle (Figs. 6, 7). Urban bare land was characterized with higher  $\text{NO}_3^-$ -N flux in surface soil and greater  $\text{NO}_3^-$ -N loss via surface runoff by the WIND, which is coincident to greater  $\text{NO}_3^-$ -N export via surface runoff from urban subwatersheds ( $2.49 \pm 0.35 \text{ mg N L}^{-1}$ ) than forest ones ( $1.10 \pm 0.45 \text{ mg N L}^{-1}$ ) in the Jiulong river watershed, Fujian, China (Huang et al., 2018b). Shi et al. (2019) also confirmed that inorganic N export to waterways was often enhanced by land use change due to urbanization, up to  $15.6 \text{ mg N L}^{-1}$  in the Wei river watershed, northwest China. Upland agriculture with fertilization also exported considerable  $\text{NO}_3^-$ -N in surface water. With the WIND simulation in the studied watershed, farmland with fertilization, mainly agricultural uplands, had a comparable pool size between  $\text{NO}_3^-$ -N and  $\text{NH}_4^+$ -N (medians at 875 and 755  $\text{kg N ha}^{-1}$  in 2013-2017, respectively) but with considerable  $\text{NO}_3^-$ -N loss via surface runoff from its surface soil (averagely  $86 \text{ kg N ha}^{-1} \text{ yr}^{-1}$  and 12.4% of ATIN pool, Figs. 6, 7). It is comparable but greater than  $\text{NO}_3^-$ -N loss via surface runoff in Baltimore LTER watershed, USA where average output at  $39 \text{ kg N ha}^{-1} \text{ yr}^{-1}$  was observed (Kaushal et al., 2008).

Considerable surface runoff losses of  $\text{NH}_4^+$ -N from surface soil of agricultural land have also been observed:  $2.87 \text{ mg N L}^{-1}$  in an agricultural subwatershed (Heidingzi) of the Songhua river, Jilin Province, China (Zhao et al., 2017),  $0.53 \pm 0.6 \text{ mg N L}^{-1}$  in agricultural subwatersheds of Jiulong river, Fujian Province, China (Huang et al., 2018b), and  $1.8 \text{ mg N L}^{-1}$  in an agricultural catchment of the Lake Poyang watershed, Jiangxi Province, China (Tang et al., 2008). The simulation in the studied watershed, interestingly, indicated that despite surface soil of farmland and forest land having comparable daily  $\text{NH}_4^+$ -N pool sizes (1825 day medians of 755  $\text{kg N km}^{-2}$  and 875  $\text{kg N km}^{-2}$  respectively yet farmland had less  $\text{NH}_4^+$ -N loss via surface runoff at  $75 \text{ kg N ha}^{-1} \text{ yr}^{-1}$  (10.8% of ATIN pool) than forest land ( $94 \text{ kg N ha}^{-1} \text{ yr}^{-1}$  and 34.9% of ATIN pool, averages of 1825 days, Figs. 6, 7). This was double the flux from urban bare land. We observed that inorganic N in stream water of the studied watershed was dominated by  $\text{NH}_4^+$ -N back to 2012 (Gao et al., 2013) when the watershed (with over 45% forest coverage) had experienced an escalating urbanization.

Interactions between pools and losses of inorganic N in surface soil are multifactor dependent but mainly driven by microbial processes in soil and soil-plant root interface (Buckeridge and Jefferies, 2007; Zhang et al., 2016; Zhang et al., 2018). Most process-based soil N cycling models fixed the microbial process rates or were considered only as a parameter (Li et al., 2000; Arnold et al., 2012; Oulehle et al., 2012). In this study, a new approach of measuring rates of soil N processes was employed and enable to provide “real” process-based simulation for N cycling in

surface soil under various land use types, especially for denitrification including both  $N_2$  and  $N_2O$  fluxes (Fig. 6). With the WIND model, a clear pattern differed among three land use types in the period of 2013-2017, i.e. daily N cycling in farmland surface soil predominantly driven by mineralization, nitrification, and volatilization while daily soil N cycling was dominated by mineralization for forest land and by both mineralization and nitrification for urban bare land (Fig. 6). The simulated mineralization rates in surface soil of the studied watershed, a subtropical zone, were comparable to the rates in agricultural lands of southwestern Spain (Vazquez et al., 2019), in the 65 arable cropping field experiments in France (Clivot et al., 2017), and in forest lands in Alberta, Canada (Lang et al., 2019) and in subtropical Australia (Zhang et al., 2018) (Table 2). Meanwhile, net soil nitrification rate in farmland by the WIND simulation in this study ranged from  $8.36-116.96 \text{ kg N km}^{-2} \text{ day}^{-1}$  (equivalent to  $0.10-0.88 \text{ mg N kg}^{-1} \text{ day}^{-1}$ ), comparable to the rates of paddy soils ( $0.36-0.48 \text{ mg N kg}^{-1} \text{ day}^{-1}$ ) in Jiangxi, China (Yang et al., 2018). However, the simulated nitrification rate in surface soils of forest and urban bare lands was less than rates of corresponding land uses in Minhang District, Shanghai, China (Yan et al., 2019) and in Archipelago, Japan (Urakawa et al., 2015). Given that net denitrification rate was calculated by the sum of  $N_2+N_2O-N$  in this study, the simulated net denitrification rate in surface soil of urban bare land and forest land were greater than those in Xiamen by measuring  $N_2O-N$  alone (urban soil:  $0.08-0.46 \text{ kg N}_2\text{O-N km}^{-2} \text{ day}^{-1}$ , Xu et al., 2019) and Guangdong, China (forest soil:  $0.0001-0.003 \text{ mg kg}^{-1} \text{ day}^{-1}$ , Tang et al., 2019). But, the simulated denitrification rate in surface soil of farmland of this study was less than the Xiamen agricultural soil ( $0.6 - 444 \text{ kg N}_2\text{O-N km}^{-2} \text{ day}^{-1}$ , Xu et al., 2019) and paddy soil from Yingtan, China ( $0.33 \pm 0.08 \text{ mg N kg}^{-1} \text{ day}^{-1}$ , Lan et al., 2015). All the comparisons of inorganic N transformation rates were listed in Table 2.

Soil microbial N processes are temperature-sensitive (Guntirias et al., 2012; Sun et al., 2013) and mostly high temperature within its certain extent promotes N metabolic activity of microbes (Schimel et al., 2004). Findings from the WIND model that EnTemp by the energy - balance module was greater than AirTemp by the air temperature module (Fig. 5), by which soil temperature was consistently lower than air temperature, were confirmed by field measurements and simulations from other studies, for instance, soil temperature higher than air temperature during daylight time (Qi et al., 2019). The increment between EnTemp and AirTemp in this study differed among land use types, i.e.  $2.1 \pm 0.9^\circ\text{C}$  for forest land,  $6.3 \pm 3.5^\circ\text{C}$  for farmland, and  $7.2 \pm 3.3^\circ\text{C}$  for urban bare land, all greater than that in surface soil (5-10 cm) of the Choptank River watershed, Maryland, USA ( $0.4$  to  $1.1^\circ\text{C}$ , averagely  $0.6 \pm 0.2^\circ\text{C}$ , Qi et al., 2019) (Table 2). On the other hand, differences of daily soil temperature among land use types found in this study, for example,  $0.2$  to  $18^\circ\text{C}$  and averagely  $5^\circ\text{C}$  between forest land and urban bare land, were coincident to the simulated daily soil

surface temperature increments between forest land and bare land in Albertville, Minnesota, USA by the energy balance (-1 - 12°C, [Herb et al., 2008](#)). The temperature increments between vegetated and bare soil is determined by short wave length radiation which is blocked by vegetation ([Herb et al., 2008](#); [Ni et al., 2019](#)). Findings from this study and others suggest that the energy-balance simulation might be appropriate for surface soil temperature rather than the air temperature module. Meanwhile, the energy balance module for surface soil temperature includes soil moisture as an important factor, which is highly determined by soil water holding capacity ([Chen et al., 2007](#)). In this study, the forest soil had higher moisture than urban bare soil because of larger soil water holding capacity ([Fig. 4](#)). On the other hand, soil moisture is influenced by land slope, a hydrological factor, which determines surface runoff and water infiltration under various land coverage ([Table S1](#)). A negative relationship between soil moisture and land slope has been reported in few studies, including farmland and forest land of hilly Jiegou catchment in Shanxi, China ([Yu et al., 2018](#)) and Yan River catchment in Shanxi, China ([Yang et al., 2017](#)). This study also demonstrated the negative relationship between soil moisture and land slope which was influenced by daily rainfall volume ([Fig. 4](#)). Evapotranspiration by vegetation is another important pathway influencing soil moisture ([Gómez-Plaza et al., 2001](#); [Ni et al., 2019](#)). The forest land and farmland in this study had greater soil moisture in surface soil than urban bare soil even though forest land had the greatest land slope ([Fig. 4](#)). The findings of the present study suggest that soil moisture is strongly determined by water holding capacity instead of land slope and vegetation (land cover). However, land slope critically determined surface runoff and infiltration of water as well as N movement ([Zhu et al., 2018](#)).

As a model, the WIND model has its assumptions and limitations. The WIND only estimates inorganic N dynamics in surface soil and does not touch organic N speciation because most N losses are inorganic forms via surface runoff (and surface soil erosion) and gaseous emissions. Therefore, organic N cycling and N dynamics in subsurface soil are not considered, which is one of the limitations for the WIND model. Meanwhile, the slope introduction to soil moisture simulation is specific to a mountainous watershed or catchment as this study explored that the slope effect on soil moisture and associated N transformation becomes evident at a steepness above 15 degree and varies by vegetation covers ([Fig. 3](#)). It suggests that in a flat watershed or catchment, the WIND might have similar estimates as other models which consider solar radiation for soil moisture simulation. At last, the current study successfully testified the WIND model differentiating the land use types on inorganic N cycling processes, but scaling these results up to a watershed or catchment should considered more aspects of various land use patches, such as exposure and length of slope, and inter- and intra- drainage networks. In short, the WIND model also requires a

conditional application as other models.

## 5. Conclusions

Land use type shifts soil N cycling due to its effects on altering soil temperature and moisture. For an urbanizing case study watershed, the WIND model which included an energy-balanced soil temperature module (EnTemp) and slope-introduced soil moisture module (SMoist) clearly illustrated the differences of inorganic N pools, and N transformation rates and pathways in surface soil under three land uses (Figs. 6, 7). Influences of soil temperature, soil moisture, and land slope on inorganic N pools were also testified and clarified using the WIND model for forest land, farmland, and urban bare land (Figs. 4, 5). Besides giving better simulation on watershed N cycling, findings from the modelling will assist strategies for watershed N management under climate changes. Although some uncertainties should be considered for this study, hopefully, these findings of the WIND might also be useful to constrain parameterization of SWAT and AGNPS and the other catchment nutrient models, such as that the energy balanced simulation might be appropriate for surface soil temperature rather than the air temperature module.

## Acknowledgements

Authors thank the staff at the Centre for Instruments, Institute of Urban Environment, Chinese Academy of Sciences for helps. This study is financially supported by the National Natural Science Foundation of China (NSFC, No. 41571483, 41661144033, 71961137007, 41807494, 41701549, 41371474).

## References

- Agehara, S., Warncke, D.D., 2005. Soil moisture and temperature effects on nitrogen release from organic nitrogen sources. *Soil Sci. Soc. Am.* 69, 1844-1855.  
<https://doi.org/10.2136/sssaj2004.0361>
- Ahmed, I.U., Mengistie, H.K., Godbold, D.L., Sanden, H., 2019. Soil moisture integrates the influence of land-use and season on soil microbial community composition in the Ethiopian highlands. *App. Soil Ecol.* 135, 85-90.  
<https://doi.org/10.1016/j.apsoil.2018.11.010>
- Allen, R.G., Pereira, L.S., Raes, D., Smith, M., 1998. Crop evapotranspiration - Guidelines for computing crop water requirements. *Food Agr. Organ. Unit. Nation.* 300 (9), D05109.
- Arnold, J.G., Moriasi, D.N., Gassman, P.W., Abbaspour, K.C., White, M.J., 2012. SWAT: model use, calibration, and validation. *Trans. Asabe* 55 (4), 1345-1352.  
<https://doi.org/10.13031/2013.42246>
- Bai, Y.Y., Scott, T.A., Min, Q.W., 2014. Climate change implications of soil

- temperature in the Mojave Desert, USA. *Front. Earth Sci.* 8 (2), 302-308.  
<https://doi.org/10.1007/s11707-013-0398-3>
- Berg, A., Lintner, B.R., Findell, K.L., Malyshev, S., Loikith, P.C., Gentine, P., 2014. Impact of soil moisture – atmosphere interactions on surface temperature distribution. *J. Clim.* 27 (21), 7976-7993. <https://doi.org/10.1175/jcli-d-13-00591.1>
- Buckeridge, K.M., Jefferies, R.L., 2007. Vegetation loss alters soil nitrogen dynamics in an Arctic salt marsh. *J. Ecol.* 95 (2), 283-293. <https://doi.org/10.1111/j.1365-2745.2007.01214.x>
- Butterbach-Bahl, K., Baggs, E.M., Dannenmann, M., Kiese, R., Zechmeister-Boltenstern, S., 2013. Nitrous oxide emissions from soils: how well do we understand the processes and their controls? *Philos. Trans. R. Soc. B-Biol. Sci.* 368 (1621), 20130122. <https://doi.org/10.1098/rstb.2013.0122>
- Cai, J.B., Liu, Y., Lei, T.W., Pereira, L.S., 2007. Estimating reference evapotranspiration with the FAO Penman-Monteith equation using daily weather forecast messages. *Agr. Forest Meteorol.* 145 (1), 22-35.  
<https://doi.org/10.1016/j.agrformet.2007.04.012>
- Costa, D., Baulch, H., Elliott, J., Pomeroy, J., Wheeler, H., 2020. Modelling nutrient dynamics in cold agricultural catchments: A review. *Environ. Modell. Softw.* 124,104586. <https://doi.org/10.1016/j.envsoft.2019.104586>
- Chen, L.D., Huang, Z.L., Gong, J., Fu, B.J., Huang, Y.L., 2007. The effect of land cover/vegetation on soil water dynamic in the hilly area of the loess plateau, China. *Catena* 70 (2), 200-208. <https://doi.org/10.1016/j.catena.2006.08.007>
- Chen, S.K., Liu, C.W., 2002. Analysis of water movement in paddy rice fields (I) experimental studies. *J. Hydrol.* 260 (1), 206-215. [https://doi.org/10.1016/s0022-1694\(01\)00615-1](https://doi.org/10.1016/s0022-1694(01)00615-1)
- Clivot, H., Mary, B., Valé, M., Cohan, J.P., Justes, E., 2017. Quantifying in situ and modeling net nitrogen mineralization from soil organic matter in arable cropping systems. *Soil Biol. Biochem.* 111, 44-59.  
<https://doi.org/10.1016/j.soilbio.2017.03.010>
- Congreves, K.A., Dutta, B., Grant, B.B., Smith, W.N., Desjardins, R.L., Wagner-Riddle, C., 2016. How does climate variability influence nitrogen loss in temperate agroecosystems under contrasting management systems? *Agr. Ecosyst. Environ.* 227, 33-41. <https://doi.org/10.1016/j.agee.2016.04.025>
- Ehrenfeld J.G., Yu S., 2012. Patterns of nitrogen mineralization in wetlands of the New Jersey Pinelands along a shallow water table gradient. *Am. Midl. Nat.* 167, 322-335. <https://doi.org/10.1674/0003-0031-167.2.322>
- Fox, D.M., Bryan, R.B., Price, A.G., 1997. The influence of slope angle on final infiltration rate for interrill conditions. *Geoderma* 80 (s 1-2), 181-194.

- [https://doi.org/10.1016/S0016-7061\(97\)00075-X](https://doi.org/10.1016/S0016-7061(97)00075-X)
- Galloway, J.N., Cowling, E.B., 2002. Reactive nitrogen and the world: 200 years of change. *Ambio: J. Human Environ.* 31 (2), 64-71. <https://doi.org/10.1579/0044-7447-31.2.64>
- Gao, J.B., Wu, Q., Li, Q.L., Ma, J., Xu, Q.F., Groffman, P.M., Yu, S., 2013. Preliminary results from monitoring of stream nitrogen concentrations, denitrification and nitrification potentials in an urbanizing watershed in Xiamen, Southeast China. *Int. J. Sust. Dev. World Ecol.* 20 (3), 223-230. <https://doi.org/10.1080/13504509.2013.782905>
- Gómez-Plaza, A., Mart, M., Albaladejo, J., Castillo, V.M., 2001. Factors regulating spatial distribution of soil water content in small semiarid catchments. *J. Hydrol.* 253 (1-4), 211-226. [https://doi.org/10.1016/S0022-1694\(01\)00483-8](https://doi.org/10.1016/S0022-1694(01)00483-8)
- Groffman, P.M., Boulware, N.J., Zipperer, W.C., Pouyat, R.V., 2002. Soil nitrogen cycle processes in urban riparian zones. *Environ. Sci. Technol.* 36 (21), 4547-4552. <https://doi.org/doi:10.1021/es020649z>
- Guntiñas, M.E., Leiros, M.C., Trasar-Cepeda, C., Gil-Sotres, F., 2012. Effects of moisture and temperature on net soil nitrogen mineralization: A laboratory study. *Eur. J. Soil Biol.* 48 (1), 73-80. <https://doi.org/10.1016/j.ejsobi.2011.07.015>
- Hauser, M., Orth, R., Seneviratne, S.I., 2016. Role of soil moisture versus recent climate change for the 2010 heat wave in Russia. *Geophys. Res. Lett.* 43, 2819-2826. <https://doi.org/10.1002/2016GL068036>
- Herb, W.R., Janke, B., Mohseni, O., Stefan, H.G., 2008. Ground surface temperature simulation for different land covers. *J. Hydrol.* 356 (3), 327-343. <https://doi.org/10.1016/j.jhydrol.2008.04.020>
- Huang, J.C., Arhonditsis, G.B., Gao, J.F., Kim, D.K., Dong, F.F., 2018a. Towards the development of a modeling framework to track nitrogen export from lowland artificial watersheds (polders). *Water Res.* 133, 319-337. <https://doi.org/10.1016/j.watres.2018.01.011>
- Huang, J.C., Gao, J.F., Yan, R.H., 2016. A phosphorus dynamic model for lowland polder systems (PDP). *Ecol. Eng.* 88, 242-255. <https://doi.org/10.1016/j.ecoleng.2015.12.033>
- Huang, K., Zhuang, G., Chang, X.U., Ying, W., Tang, A., 2008. The chemistry of the severe acidic precipitation in Shanghai, China. *Atmos. Res.* 89 (1), 149-160. <https://doi.org/10.1016/j.atmosres.2008.01.006>
- Huang, Y., Huang, J., Ervinia, A., Duan, S., Kaushal, S., 2018b. Land use and climate variability amplifies watershed nitrogen exports in coastal China. *Ocean Coastal Manage.*, <https://doi.org/10.1016/j.ocecoaman.2018.1002.1024>.
- Kaushal, S.S., Groffman, P.M., Band, L.E., Elliott, E.M., Shields, C.A., Carol, K., 2011. Tracking nonpoint source nitrogen pollution in human-impacted

- watersheds. *Environ. Sci. Technol.* 45 (19), 8225-8232.  
<https://doi.org/10.1021/es200779e>
- Kaushal, S.S., Groffman, P.M., Band, L.E., Shields, C.A., Morgan, R.P., Palmer, M.A., Belt, K.T., et al., 2008. Interaction between urbanization and climate variability amplifies watershed nitrate export in Maryland. *Environ. Sci. Technol.* 42 (16), 5872-5878. <https://doi.org/10.1021/es800264f>
- Kettridge, N.B., Baird, A.A., 2008. Modelling soil temperatures in northern peatlands. *Eur. J. Soil Biol.* 59 (2), 327-338. <https://doi.org/10.1111/j.1365-2389.2007.01000.x>
- Kwon, Y.H., Koo, B.K., 2017. Development and evaluation of the Soil and Water Temperature Model (SWTM) for rural catchments. *J. Hydrol.* 553, 457-470.  
<https://doi.org/10.1016/j.jhydrol.2017.08.017>
- Lan, T., Yong, H., Cai, Z., 2015. Denitrification and its product composition in typical Chinese paddy soils. *Biol. Fert. Soil.* 51 (1), 89-98.  
<https://doi.org/10.1007/s00374-014-0953-4>
- Lang, M., Li, P., Ti, C., Zhu, S., Chang, S.X., 2019. Soil gross nitrogen transformations are related to land-uses in two agroforestry systems. *Ecol. Eng.* 127, 431-439. <https://doi.org/10.1016/j.ecoleng.2018.12.022>
- Li, C., Aber, J., Stange, F., Butterbach-Bahl, K., Papen, H., 2000. A process-oriented model of N<sub>2</sub>O and NO emissions from forest soils: Model development. *J. Geophys. Res. Atmos.* 105 (D4), 4369-4384.  
<https://doi.org/10.1029/1999JD900949>
- Li, Z., Luo, C., Xi, Q., Li, H., Pan, J., Zhou, Q., Xiong, Z., 2015. Assessment of the AnnAGNPS model in simulating runoff and nutrients in a typical small watershed in the Taihu Lake basin, China. *Catena* 133 (20), 349-361.  
<https://doi.org/10.1016/j.catena.2015.06.007>
- Lin, X.D., Yu, S., Ma, H.W., 2018. Integrative application of life cycle assessment and risk assessment to environmental impacts of anthropogenic pollutants at a watershed scale. *B. Environ. Contam. Tox.* 100, 41-48.  
<https://doi.org/10.1007/s00128-017-2257-5>
- Lu, M.C., Chang, C.T., Lin, T.C., Wang, L.J., Wang, C.P., Hsu, T.C., Huang, J.C., 2017. Modeling the terrestrial N processes in a small mountain catchment through INCA-N: A case study in Taiwan. *Sci. Total Environ.* 593-594, 319-329.  
<https://doi.org/10.1016/j.scitotenv.2017.03.178>
- Matinzadeh, M.M., Koupai, J.A., Sadeghi-Lari, A., Nozari, H., Shayannejad, M., 2017. Development of an innovative integrated model for the simulation of nitrogen dynamics in farmlands with drainage systems using the system dynamics approach. *Ecol. Model.* 347, 11-28.  
<https://doi.org/10.1016/j.ecolmodel.2016.12.014>

- Morugan-Coronado, A., Garcia-Orenes, F., Mcmillan, M., Pereg, L., 2019. The effect of moisture on soil microbial properties and nitrogen cyclers in Mediterranean sweet orange orchards under organic and inorganic fertilization. *Sci. Total Environ.* 622, 158-167. <https://doi.org/10.1016/j.scitotenv.2018.11.174>
- Nanda, A., Sen, S., McNamara, J.P., 2019. How spatiotemporal variation of soil moisture can explain hydrological connectivity of infiltration-excess dominated hillslope: Observations from lesser Himalayan landscape. *J. Hydrol.* 579, 124146. <https://doi.org/10.1016/j.jhydrol.2019.124146>
- Ni, J.J., Cheng, Y.F., Wang, Q.H., Ng, C.W.W., Garg, A., 2019. Effects of vegetation on soil temperature and water content: Field monitoring and numerical modelling. *J. Hydrol.* 212, 226-231. <https://doi.org/10.1016/j.jhydrol.2019.02.009>
- Oulehle, F., Cosby, B.J., Wright, B.F., Hruška, J., Kopáček, J., Kram, P., Evans, C.D., et al., 2012. Modelling soil nitrogen: The MAGIC model with nitrogen retention linked to carbon turnover using decomposer dynamics. *Environ. Pollut.* 165, 158-166. <https://doi.org/10.1016/j.envpol.2012.02.021>
- Qi, J., Zhang, X., Cosh, M.H., 2019. Modeling soil temperature in a temperate region: A comparison between empirical and physically based methods in SWAT. *Ecol. Eng.* 129, 134-143. <https://doi.org/10.1016/j.ecoleng.2019.01.017>
- Qiu, Y., Fu, B.J., Wang, J., Chen, L.D., 2001. Soil moisture variation in relation to topography and land use in a hillslope catchment of the Loess Plateau, China. *J. Hydrol.* 240 (3-4), 243-263. [https://doi.org/10.1016/s0022-1694\(00\)00362-0](https://doi.org/10.1016/s0022-1694(00)00362-0)
- Romano, E., Giudici, M., 2009. On the use of meteorological data to assess the evaporation from a bare soil. *J. Hydrol.* 372 (1), 30-40. <https://doi.org/10.1016/j.jhydrol.2009.04.003>
- Schimel, J.P., Bilbrough, C., Welker, J.M., 2004. Increased snow depth affects microbial activity and nitrogen mineralization in two Arctic tundra communities. *Soil Biol. Biochem.* 36 (2), 217-227. <https://doi.org/10.1016/j.soilbio.2003.09.008>
- Shi, P., Zhang, Y., Song, J.X., Li, P., Wang, Y.S., Zhang, X.M., B, L.Z., et al., 2019. Response of nitrogen pollution in surface water to land use and social-economic factors in the Weihe River watershed, northwest China. *Sustain. Cities. Soc.* 50, 101658. <https://doi.org/10.1016/j.scs.2019.101658>
- Stieglitz, M., Shaman, J., McNamara, J., Engel, V., Shanley, J., Kling, G.W., 2003. An approach to understanding hydrologic connectivity on the hillslope and the implications for nutrient transport. *Global Biogeochem. Cy.* 17 (4), 1105. <https://doi.org/10.1029/2003GB002041>
- Sun, S., Liu, J., Chang, S.X., 2013. Temperature sensitivity of soil carbon and nitrogen mineralization: impacts of nitrogen species and land use type. *Plant Soil* 372 (1-2), 597-608. <https://doi.org/10.1007/s11104-013-1758-1>

- Tang, J.L., Zhang, B., Chao, G., Zepp, H., 2008. Hydrological pathway and source area of nutrient losses identified by a multi-scale monitoring in an agricultural catchment. *Catena* 72 (4), 374-385. <https://doi.org/10.1016/j.catena.2007.07.004>
- Tang, Y., Yu, G., Zhang, X., Wang, Q., Tian, D., Tian, J., Niu, S., et al., 2019. Environmental variables better explain changes in potential nitrification and denitrification activities than microbial properties in fertilized forest soils. *Sci. Total Environ.* 647 (3), 653-662. <https://doi.org/10.1016/j.scitotenv.2018.07.437>
- Urakawa, R., Ohte, N., Shibata, H., Tateno, R., Hishi, T., Fukushima, K., Inagaki, Y., et al., 2015. Biogeochemical nitrogen properties of forest soils in the Japanese archipelago. *Ecol. Res.* 30 (1), 1-2. <https://doi.org/10.1007/s11284-014-1212-8>
- Vaezi, A.R., Zarrinabadi, E., Auerswald, K., 2017. Interaction of land use, slope gradient and rain sequence on runoff and soil loss from weakly aggregated semi-arid soils. *Soil Tillage Res.* 172, 22-31. <https://doi.org/10.1016/j.still.2017.05.001>
- Vazquez, E., Benito, M., Espejo, R., Teutschero, N., 2019. Effects of no-tillage and liming amendment combination on soil carbon and nitrogen mineralization. *Eur. J. Soil Biol.* 93, 103090. <https://doi.org/10.1016/j.ejsobi.2019.103090>
- Vitousek, P.M., Howarth, R.W., 1991. Nitrogen limitation on land and in the sea: How can it occur? *Biogeochemistry* 13 (2), 87-115. <https://doi.org/10.1007/BF00002772>
- Wade, A.J., Durand, P., Beaujouan, V., Wessel, W.W., Raat, K.J., Whitehead, P.G., Butterfield, D., et al., 2002. A nitrogen model for European ecosystems: INCA, new model structure and equations. *Hydrol. Earth Syst. Sci.* 6 (3), 559-582. <https://doi.org/10.5194/hess-6-559-2002>
- Wu, L., Peng, M.L., Qiao, S.S., Ma, X.Y., 2018. Assessing impacts of rainfall intensity and slope on dissolved and adsorbed nitrogen loss under bare loessial soil by simulated rainfalls. *Catena* 170, 51-63. <https://doi.org/10.1016/j.catena.2018.06.007>
- Xiao, H.Y., Tang, C.G., Xiao, H.W., Liu, X.Y., Liu, C.Q., 2010. Mosses indicating atmospheric nitrogen deposition and sources in the Yangtze River drainage basin, China. *J. Geophys. Res. Atmos.* 115 (D14), 1307-1314. <https://doi.org/10.1029/2009JD012900>
- Xu, H.J., Yang, X.R., Li, S., Xue, X.M., Chang, S., Li, H., Singh, B.K., et al., 2019. Nitrogen inputs are more important than denitrifier abundances in controlling denitrification-derived N<sub>2</sub>O emission from both urban and agricultural soils. *Sci. Total Environ.* 650 (Pt 2), 2807-2817. <https://doi.org/10.1016/j.scitotenv.2018.10.001>
- Yan, L.B., Xie, C.K., Xu, X., Che, S.Q., 2019. Effects of revetment type on the spatial distribution of soil nitrification and denitrification in adjacent tidal urban riparian zones. *Ecol. Eng.* 132, 65-74. <https://doi.org/10.1016/j.ecoleng.2019.04.005>

- Yang, Y., Dou, Y., Dong, L., An, S., 2017. Spatial pattern and heterogeneity of soil moisture along a transect in a small catchment on the Loess Plateau. *J. Hydrol.* 550, 466-477. <https://doi.org/10.1016/j.jhydrol.2017.05.026>
- Yang, Y.J., Zhang, H.P., Shan, Y.H., Wang, J.J., Cai, Z.C., 2018. Response of denitrification in paddy soils with different nitrification rates to soil moisture and glucose addition. *Sci. Total Environ.* 651, 2097-2104. <https://doi.org/10.1016/j.scitotenv.2018.10.066>
- Yu, B.W., Liu, G.H., Liu, Q.S., Wang, X.P., Feng, J.L., Huang, C., 2018. Soil moisture variations at different topographic domains and land use types in the semi-arid Loess Plateau, China. *Catena* 165, 125-132. <https://doi.org/10.1016/j.catena.2018.01.020>
- Yu, S., Ehrenfeld, J.G., 2010. Relationships among plants, soils and microbial communities along a hydrological gradient in the New Jersey Pinelands, USA. *Ann. Bot.* 105, 185-196. <https://doi.org/10.1093/aob/mcp183>
- Zhang, J.B., Peng, T., Tang, J.L., Lei, Y., Yun, K., Cai, Z.C., Bo, Z., et al., 2016. The characteristics of soil N transformations regulate the composition of hydrologic N export from terrestrial ecosystem: Soil N cycle regulate hydrologic N loss. *J. Geophys. Res. Biogeo.* 121 (6), 1409-1419. <https://doi.org/10.1002/2016JG003398>
- Zhang, M.Y., Wang, W.J., Wang, D.J., Heenan, M., Xu, Z.H., 2018. Short-term responses of soil nitrogen mineralization, nitrification and denitrification to prescribed burning in a suburban forest ecosystem of subtropical Australia. *Sci. Total Environ.* 642, 879-886. <https://doi.org/10.1016/j.scitotenv.2018.06.144>
- Zhao, G.J., Hörmann, G., Fohrer, N., Li, H.P., Gao, J.F., Tian, K., 2011. Development and application of a nitrogen simulation model in a data scarce catchment in South China. *Agr. Water Manage.* 98 (4), 619-631. <https://doi.org/10.1016/j.agwat.2010.10.022>
- Zhao, Q., Chang, D., Wang, K., Huang, J., 2017. Patterns of nitrogen export from a seasonal freezing agricultural watershed during the thawing period. *Sci. Total Environ.* 599–600, 442-450. <https://doi.org/10.1016/j.scitotenv.2017.04.174>
- Zhu, Q., Castellano, M.J., Yang, G.S., 2018. Coupling soil water processes and the nitrogen cycle across spatial scales: Potentials, bottlenecks and solutions. *Earth-Sci. Rev.* 187, 248-258. <https://doi.org/10.1016/j.earscirev.2018.10.005>

**Table 1**  
Sources of parameters and datasets used for the Watershed Inorganic Nitrogen Dynamic (WIND) Model.

Item	Description	Data Source
Land use type	Satellite image interpretation (Landsat 7 ETM+ in August 2010) using ArcGIS	Geospatial Data Cloud Site ( <a href="http://www.gscloud.cn">http://www.gscloud.cn</a> )
Land elevation and slope	Digital elevation model (ASTGTM2_N24E118) using ArcGIS	Geospatial Data Cloud Site ( <a href="http://www.gscloud.cn">http://www.gscloud.cn</a> )
Temperature, solar radiation, rainfall, relative humidity, wind speed, etc.	Soil temperature simulation	National Meteorological Information Center ( <a href="http://data.cma.cn">http://data.cma.cn</a> )
Parameters for evapotranspiration, potential evaporation, surface runoff and infiltration rate	Soil moisture partitioning	Published literature, e.g. Allen et al. (1998), Chen et al. (2002), Cai et al. (2007) and Huang et al. (2016)
Contents of moisture, ammonia and nitrate in soil and soil bulk density	Calibration and validation of the WIND model for moisture and inorganic N in surface soil	Two sampling events of surface soil in the studied watershed in 2013 and 2016/17 and measurements of this study
Rates of N cycling processes, i.e. mineralization, nitrification, denitrification, filtration, and volatilization etc.	Parameters of the WIND model for soil N cycling processes	Measurements of the sampling event in 2016/17 of this study and published literature, e.g. Wade et al. (2002), Zhao et al. (2011), and Lu et al. (2017)
Atmospheric N deposition rate and fertilization rate	Parameters of the WIND model for soil N inputs	Published literature, e.g. Huang et al. (2018), Xiao et al. (2010) and Huang et al. (2008)

**Table 2**  
Comparisons of rates of soil N cycling processes and soil temperature increment (against to air-temperature based empirical simulation of soil temperature) between the WIND simulation and the published literature. Rate units of the measurements in this study have been converted into the same as the literature ones.

Parameter	Time resolution	Land use	Simulated	Published	Unit	Source
Mineralization	Daily	Farmland	0.14 - 1.40	0.28 - 1.63	mg N kg <sup>-1</sup> day <sup>-1</sup>	Vazquez et al. (2019)
	Daily	Farmland (arable)	19 - 185	17 - 167	kg N km <sup>-2</sup> day <sup>-1</sup>	Clivot et al. (2017)
	Daily	Forest land	0.18 - 0.90	0.29 - 0.92	mg N kg <sup>-1</sup> day <sup>-1</sup>	Lang et al. (2019)
	Daily	Forest land	0.40	0.53 ± 0.08	mg N kg <sup>-1</sup> day <sup>-1</sup>	Zhang et al. (2018)
	Daily	Forest land	0.40	0.62 ± 0.68	mg N kg <sup>-1</sup> day <sup>-1</sup>	Urakawa et al. (2015)
Nitrification	Daily	Farmland (paddy soils)	0.10 - 0.88	0.36 - 0.48	mg N kg <sup>-1</sup> day <sup>-1</sup>	Yang et al. (2018)
	Daily	Forest land	0.05 - 0.27	0.07 - 0.13	mg N kg <sup>-1</sup> day <sup>-1</sup>	Tang et al. (2019)
	Daily	Forest land	0.12	0.25 ± 0.45	mg N kg <sup>-1</sup> day <sup>-1</sup>	Urakawa et al. (2015)
	Daily	Urban soil	0.21	0.25 ± 0.04	mg N kg <sup>-1</sup> day <sup>-1</sup>	Yan et al. (2019)
Denitrification	Daily	Farmland	1.7 - 11.4	0.6 - 444	kg N km <sup>-2</sup> day <sup>-1</sup>	Xu et al. (2019)
	Daily	Farmland (paddy soils)	0.03	0.33 ± 0.08	mg N kg <sup>-1</sup> day <sup>-1</sup>	Lan et al. (2015)
	Daily	Forest land	0.004 - 0.02	0.0001 - 0.003	mg N kg <sup>-1</sup> day <sup>-1</sup>	Tang et al. (2019)
	Daily	Urban soil	0.35 - 2.55	0.08 - 0.46	kg N km <sup>-2</sup> day <sup>-1</sup>	Xu et al. (2019)
Soil temperature increment	Daily	Forest land	2.1 ± 0.9		°C	
	Daily	Farmland	6.3 ± 3.5	0.4 - 1.1	°C	Qi et al. (2019)
	Daily	Urban bare land	7.2 ± 3.3	(Mean, 0.6 ± 0.2)	°C	